RSC Advances

ROYAL SOCIETY
OF CHEMISTRY

www.rsc.org/advances

RSC advances

RSC **Publishing**

ARTICLE

Largely enhanced mechanical properties and heat distortion temperature of β-nucleated isotactic polypropylene by adding ultrafine full-vulcanized powdered rubber

Yanling Zhu, Yongsheng Zhao, Sha Deng, Qin Zhang, Qiang Fu*

Abstract: In this work, ultrafine full-vulcanized powdered rubber (EA-UFPR) was incorporated into β-nucleated isotactic polypropylene (β-iPP) in order to investigate the combined effects of EA-UFPR and β-nucleation on mechanical properties and heat distortion temperature (HDT) of β-iPP. A large enhancement of toughness verified as a synergistic effect had been achieved by adding a small amount of EA-UFPR (≤ 2 wt %) into β-nucleated iPP. Decreased crystallization kinetics and even more interestingly, a transformation of crystalline morphology from β-spherulites to bundle-like β-crystals were observed as due to a possible retarded self-assembly of nucleating agent by adding small amounts of EA-UFPR. On one hand, the combined effects between EA-UFPR particles and β-crystalline morphology on promoting the plastic deformation of matrix play important roles in enhancing the toughness. On the other hand, a unique interconnected structure as composed by the bundle-like crystals and dispersed EA-UFPR particles was proposed for the improvement in impact strength and HDT. Our work provides a new way to control crystalline morphology and largely improve the toughness and heat distortion temperature of iPP, which are particularly important for the industrial application of iPP.

Keywords: mechanical properties, heat distortion temperature, crystallization behaviour, crystalline morphology

1. Introduction

There are at least four different crystalline forms presented in isotactic polypropylene: monoclinic α-form, trigonal β-form, orthorhombic γ-form[1] and mesomorphic smectic form.[2,3] Compared with other crystalline structures, β-modified isotactic polypropylene (β-iPP) has attracted scientific and industrial attention for its improved elongation at break and excellent notched izod impact strength owning to micromechanical mechanism initiated within intercrystalline amorphous phase and β-α morphological transition.[4-6] Another merit of β-iPP is its much higher heat distortion temperature compared with α-PP, which is also important for the industry application of iPP.[7] The β-form is a thermodynamically metastable phase, which can be obtained by special conditions, such as blending with nucleating agents,[8] temperature gradient,[9] or shear.[10-12] Compared with other methods, blending with β-nucleating agent is the most effective and accessible method to obtain high β-form content in iPP. A large amount of researches has demonstrated that the toughness of β-iPP is proportional to the β-form concentration.[13] Nevertheless, the β-crystal concentration is not the only factor influencing the impact strength of iPP, the β-nucleated crystalline morphology also plays an important role in tuning toughness of iPP.[14] Three types of β-crystalline morphologies,

namely, β-spherulite, β-transcrystalline entity, and "flower"-like agglomerate of β-crystallites, were reported in our group via increasing the final molten temperature (T_f).[15] Super tensile elongation was observed for the sample with "flower-like" agglomerate sample due to its sufficient connection between the crystallites. Although it is indeed helpful for toughness enhancement to transform primary α form into a crystalline morphology dominated by β crystals, the efficiency and the degree of improvement is still limited, and a saturated enhancement is often observed. .

Ultrafine full-vulcanized powdered rubber (UFPR), a new kind of highly cross-linked nano-particle rubbers, can be prepared by using rubber latex with irradiation sensitives as raw material followed by irradiation cross-linking and spray drying before obtaining full vulcanized powdered rubber with the diameter of 30nm~100nm.[16] It has been proved that the addition of UFPR can greatly improve the toughness of many plastics, and at the same time it can keep the stiffness and/or heat resistance constant instead of deteriorating.[17, 18] Qiao et al. investigated the effect of UFPR on mechanical properties of polypropylene, and their results showed that the impact strength and the tensile strength could be improved simultaneously by adding a small amount of EA-UFPR (<5 wt %).[19] Moreover, Zhao et al.

found that the elongation of PLLA could be enhanced from 6% to 230% by using 3 wt% of EA-UFPR, and the tensile strength keeps unchanged.[20] Very interestingly, similar to the addition of β-nucleating agent, a much improved heat distortion temperature of iPP can be also achieved by adding of UFPR.[19] However, there is a saturated enhancement in toughness or heat distortion temperature of samples with adding UFPR, and a deteriorated property is usually observed with further increasing of UFPR content.

Since the toughness and heat distortion temperature are the main properties for the application of iPP, while adding β-nucleating agent or UFPR alone into iPP usually results in a saturated properties enhancement. In this work, a small amount of UFPR was incorporated into β-iPP to further improve the toughness and heat distortion temperature of iPP. Our goals are two folds. The one is to investigate the combined effects of UFPR and β-nucleation on the toughness and heat distortion temperature of iPP, and the other is to explore the influence of UFPR on the crystallization kinetics and crystalline morphology of β nucleated isotactic polypropylene (β-iPP).

2. Experimental section

2.1 Materials and sample preparation

Commercially available isotactic polypropylene, model T30S, was purchased from Dushanzi Petroleum Chemical Co. China, with a melt flow rate (MFR) of 3 g/10 min (230 °C, 21.6 N), Mw= 39.9×10^4 g/mol, and M_w/M_n = 4.6. Ultrafine Full-Vulcanized Powdered Rubber denominated EA-UFPR (Narpow VP-362) with an average single particle size of about 30 nm, as shown in Fig. 1(a), was kindly supplied by Beijing BHY chemical Industry New Technology Corp. A highly active rare earth β-nucleating agent (trade name WBG), also in a powder form as shown in Fig.1(b), was provided by Guangdong Winner Functional Materials Co. (Foshan, China). An antioxidant (0.5 wt %), Irganox 1010, was added to avoid degradation during melt blending and injection molding.
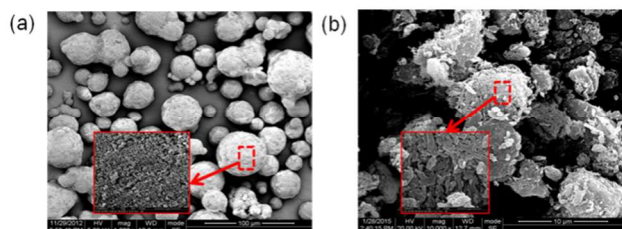
Figure 1 Micrographs for ultrafine full-vulcanized powdered rubber (EA-UFPR) and raw rare earth β-nucleating agent (WBG).

To achieve good dispersion and desired loading of β-nuclear agent, a master batch of iPP with 5 wt % WBG was prepared firstly by a TSSJ-25 co-rotating twin screw extruder (China) at a barrel temperatures ranging from 150 °C to 200 °C, and the same method was employed to prepare a master batch with 30 wt % EA-UFPR. Then, the blends were prepared by melt compounding iPP with WBG or EA-UFPR on specific proportion to obtain the corresponding blends. A saturation value not only in β crystal content but on mechanical properties was emerged with the increasing of WBG content into iPP.[21] Since adding 0.05 wt % of WBG could achieve almost 90% of β-crystal form and a saturated enhancement in toughness was observed at this point, thus in this work, the content β-nucleating agent is fixed at 0.05 wt % and the content of EA-UFPR is changed from 1 wt % to 6 wt %. After pelletizing, standard specimens were molded on an injection machine (PS40E5ASE, Japan) at barrel temperature of 200 °C and mould temperature of 30 °C. For convenience, the specimens were abbreviated I/0.05G/yR, where the I, G and R represent iPP, WBG and EA-UFPR respectively, and y indicate the content of EA-UFPR is y%. For example, I0.05G1R means iPP blend with 0.05 wt % WBG and 1 wt % EA-UFPR.

2.2 Property and structure characterization

2.2.1 Differential Scanning Calorimetry (DSC)

The isothermal crystallization was recorded by a Pekin-Elmer pyris-1 DSC (USA) under dry nitrogen atmosphere, calibrated with indium (T_m=156.6 °C, $\triangle H_m$=28.45 kJ/kg) and zinc (T_m=419.47 °C, $\triangle H_m$=108.37 kJ/kg). Aluminum capsules were employed with sample weights of approximately 5 mg. The thermal history prior to the crystallization of iPP was eliminated by keeping the samples at a temperature of 200 °C for 5 min. In order to inspect the non-isothermal crystallization behaviour of samples with various EA-UFPR contents, each specimen was cooled to 50 °C at a rate of 10 °C/min. Thereafter, the specimen was heated secondly to the melting point at a rate of 10 °C/min. Isothermal crystallization process: with removing thermal history firstly, the samples were cooled to the given T_c (138 °C) at a rate of 100 °C /min and maintained at this temperature for 30 min, and subsequently the sample was heated from 50 °C to 200 °C at a heating rate of 10 °C /min.

The degree of crystallinity (X_c) and relative fraction of β-crystals (K_β) of PP matrix are evaluated according to the most commonly adopted equation:

$$X_C = (\frac{\Delta H_\alpha}{\Delta H_\alpha^0} + \frac{\Delta H_\beta}{\Delta H_\beta^0}) \times 100\% \qquad (1)$$

$$K_\beta = \frac{\Delta H_\beta}{\Delta H_\alpha + \Delta H_\beta} \times 100\% \qquad (2)$$

Where ΔH_α and ΔH_β are the enthalpies of the melting of α crystalline phase and β crystalline phase, respectively, and ΔH_α and ΔH_β are the melting enthalpies of 100 % crystalline phase correspond to α crystal and β crystal (177 J/g for α crystal and 168.5 J/g for β crystal).

2.2.2 Wide angle X-ray diffraction (WAXD)

The WAXD spectra was acquired from a Philips X'Pert pro MPD apparatus with conventional Cu Kα X-ray (λ = 0.154 nm, reflection mode) tube at a voltage of 40 kv and a filament current of 40 mA. The scanning 2θ range was from 5 ° to 40 ° at a scanning rate of 5 °/min. Through deconvoluting the peaks of WAXD, the overall crystallinity X_c was calculated according to the following equation:

$$X_c = \frac{\sum A_{cryst}}{\sum A_{cryst} + \sum A_{amorp}} \times 100\% \quad (3)$$

Where A_{cryst} and A_{amorp} represent for the integral intensities of crystal and amorphous, respectively. The relative amount of the β-form crystal K_β was evaluated according to the method of Turner-Jones et al.[2]

$$K_\beta = \frac{A_\beta(300)}{A_\alpha(110) + A_\alpha(040) + A_\alpha(130) + A_\beta(300)} \times 100\% \quad (4)$$

$$K_\alpha = (1 - K_\beta) \times 100\% \quad (5)$$

Where $A_{\beta(300)}$ is the integral intensity of the (300) reflection peak of β-form at 2θ=16.1 °, and $A_{\alpha(110)}$, $A_{\alpha(040)}$, $A_{\alpha(130)}$ represent for the integral intensities of the (110), (040), (130) reflection peak, and the responding 2θ are 14.1 °, 16.9 °, 18.6 °, respectively.

2.2.3 Polarized optical microscope (POM)

The crystalline morphologies of samples were observed employing a Leica DMIP polarized optical microscope (POM) equipped with a Linkam THMS 600 hot stage under crossed polarizers. Small fragments of all samples were inserted between two microscope cover glasses and placed on the hot stage. The samples were melted in 200 °C for 5 min in order to erase the thermal history; subsequently, the temperature was cooled to 138 °C, and kept at this temperature for 30 min. The morphological photographs of crystallization were recorded with the aid of a digital camera during isothermal crystallization process.

2.2.4 Scanning electron microscopy (SEM)

To observe the crystalline morphology clearly, permanganic etching of the samples prior to the observation was carried out. Due to the difficulty in distinguishing the matrix and EA-UFPR, the EA-UFPR was removed by xylene at 60 °C for 20 min. The surfaces of all the samples were sputter-coated with a layer of gold to provide enhanced conductivity. Then, the test was carried out on an FEI Inspect F field emission scanning electron microscope (FE-SEM, USA) with an acceleration voltage of 20 kV.

2.2.5 Mechanical property measurements

The notched Izod impact strength was measured with a VJ-40 Izod machine according to the ASTM D256-04 standard. The measurement was carried out at every set temperature after keeping at least 2h, which was literally set as -20 °C, -10 °C, 0 °C, 10 °C, 20 °C. The average value reported was derived from at least five specimens. The tensile strength was tested at a constant temperature of 23 °C with an SANS Universal tensile testing machine controlled by a two-step program, according to the ASTM D638-03 standard.

2.2.6 Heat distortion temperature

Heat distortion temperature (HDT), at which the materials deflects by 0.25 mm at an applied force, was measured in three-point blending mode using a HDT/VICAT heat distortion tester according to ASTM D648 standard. The specimens were tested under a stress of 0.455 MPa from room temperature to 160 °C at a heating rate of 120 °C /h. The average value listed was derived from at least five specimens.

3. Results and discussion

3.1 Dependence of mechanical properties of β-iPP on EA-UFPR

The effect of EA-UFPR on izod impact strength of β-nucleated iPP (Ternary compounds) was measured at different temperatures and shown in Fig. 2(a). For pure β-iPP, the notched Izod impact strength calculated is about 3 kJ/m^2 at -20 °C, and remains unchanged with increasing temperature up to 0 °C, while it starts to increase to a final value of about 6.0 kJ/m^2 as the testing temperature increases to 20 °C, indicating that an enhancement in impact strength of β-nucleated iPP can be achieved above the glass transition temperature of iPP ($T_{g,iPP} \approx 0$ °C). Similar results have been extensively reported in the previous literatures.[21, 22] After adding 1 wt % EA-UFPR into β-nucleated iPP, a slight increase in notched Izod impact strength is obtained from 3.0 kJ/m^2 to 4.5 kJ/m^2 at -20 °C, while an obvious increase in impact strength is achieved that the increased value is about 2 times higher than that of pure β-iPP (from 6 kJ/m^2 to 13 kJ/m^2) at 20 °C, and similar values are observed in I0.05G2R. However, the notched Izod impact strength decreases with the further increasing of EA-UFPR content in β-iPP. When adding an excess content of EA-UFPR, taking I0.05G6R as an example, the impact strength drops significantly and reaches a value at a similar level or even lower one in comparsion with that of pure β-iPP. Overall, positive interaction between EA-UFPR and WBG can be achieved for systems with lower content of EA-UFPR such as I0.05G1R and I0.05G2R, while inter-hindered effect was enhanced and even out of control that results in a drop of impact strength for I0.05G4R and I0.05G6R. Therefore, it can be concluded that adding a small amount of EA-UFPR (less than 2 wt %) into β-nucleated iPP is enough and effective for the significant increase of impact strength, especially when the testing temperature is above the glass transition temperature of iPP.
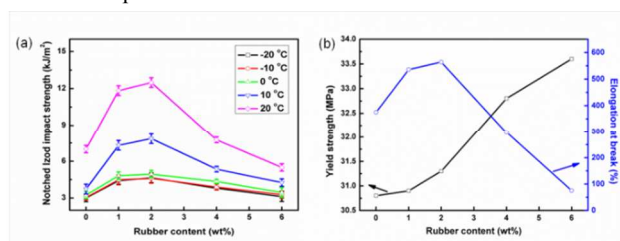
Figure 2 Composition dependence of (a) notched Izod impact strength tested at different temperatures, (b) yield strength and elongation at break at room temperature.

The tensile stress-strain behaviour is also analyzed to determinate the effect of EA-UFPR content on mechanical properties. As shown in Fig. 2(b), the tensile strength increases slightly with the increment of EA-UFPR content, whose superior feature is nano-sized particles with high degree of cross-linking, and this is totally opposite with the case of blending with other normal rubbers. The elongation at break increases significantly when the EA-UFPR content is less than 2 wt %, but it decreases obviously with the further increase in EA-UFPR content.

To analyze the interaction between EA-UFPR and β-nucleating agent on the impact strength, a linear prediction (dotted line) of the improvement in impact strength for sample I1R (iPP with only 1wt% EA-UFPR) and I0.05G (iPP with only 0.05wt % β-nucleating agent) is calculated and used to compare with that of I0.05G1R, as shown in Fig. 3(a). It should be noted that the impact strength of α-iPP is used as a base line. It is illustrated that the impact strength of I0.05G1R is higher than the linear addition of I1R and I 0.05G at all the testing temperature, indicating a synergistic effect of EA-UFPR and β-nucleating agent on the impact strength in I0.05G1R. The fracture surface of the broken specimens was examined via SEM, and the result obtained at 20 °C is taken as example and shown in Fig. 3(b). The intensity of plastic deformation increase in I0.05G compared to that of α-iPP, suggesting that β-iPP is more easily to generate shear yielding deformation in relative to α-iPP. Additionally, a large amount of microvoids resulting from interfacial debonding between iPP matrix and EA-UFPR are clearly observed for I1R, but no perceptible deformation of the matrix suggests that the α-crystalline morphology undergoes brittle failure. However, not only microvoids but also intensively shear yielding deformation appear for the sample I0.05G1R. It is suggested that the addition of EA-UFPR into β-nucleated iPP can promote the plastic deformation of iPP and then cause effective energy dissipation during impacting process, thus resulting in a large increase of impact strength.
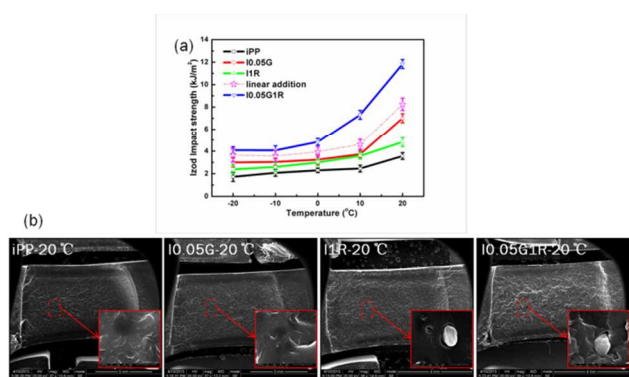
Figure 3 (a) Synergistic effects of EV-UFPR and β-NA on Izod impact strength, (b) SEM micrographs of impact fractured surfaces tested at 20 °C of the blends: iPP, I0.05G, I1R and I0.05G1R, respectively.

3.2 Effects of EA-UFPR on heat distortion temperature

It is well known that the heat distortion temperature (HDT) is a measurement of the upper boundary for the dimensional stability of a material under a specific load and temperature, and a critical parameter for product design and it is widely used in automotive applications. Hence, the HDT of the prepared samples is of particular interest and was measured in our work. Higher HDT value is desirable to attain better performance during high-temperature service conditions. As shown in Fig. 4, an enhancement in HDT is observed with the EA-UFPR content for both α-iPP and β-nucleated iPP. There also seems to be a saturated enhancement in HDT at the point with 1 wt % EA-UFPR, while no obvious increase of HDT is observed above the content. Clearly, the HDT of β-nucleated iPP is always higher than that of α-iPP at all contents of EA-UFPR, in particular for samples with 1 wt % of EA-UFPR. For example, the improvement of HDT for α-iPP is only 4 °C (from 94 °C to 98 °C) by adding1 wt % of EA-UFPR (I1R), while it becomes 10 ℃ (from 98 °C to 108 °C) for β-nucleated iPP (I0.05G1R). In this case, a synergistic effect of EA-UFPR and β-nucleating agent on HDT is also observed. It should be also noted that the value of HDT is reported in this work somewhat lower than that reported in literature.[23] This is probably attributed to the existence of core-skin structure for the lower modulus of skin region resulted from injection molding.[24] Several factors are known that can influence the HDT of polymeric materials including flexural modulus, the degree of crystallinity, T_g, thermal history[25] and the fillers.[26] The reasons for the increments in HDT of our study will be discussed below.
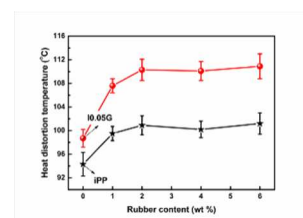
Figure 4 Effects of EA-UFPR contents and β nucleating agent on heat distortion temperature (HDT).

3.3 Crystalline morphology and crystallinity

It is very interesting to see the synergetic improvements in toughness and HDT by introducing a small amount of EA-UFPR into β-iPP. To explore the reasons for the enhancements of mechanical properties, wide-angle X-ray diffractograms were measured (Fig. 5). The relative fractions of β-crystal ($K_β$) of samples with various EA-UFPR contents were calculated (table 1). In the profile, the (110) plane at 2θ=14.1 °, (040) plane at 16.9 °, and (130) plane at 18.6 ° are the principal reflections for α crystals of PP, while (300) plane at 16.1 ° is the principle reflection of β crystals. In these patterns, the (300) reflection of β-crystal are clearly seen at about 16 ° in 2θ, and their intensities are different when changing the content of EA-UFPR. Comparing with low content of EA-UFPR, the intensity of β-crystal in I0.05G6R reduces obviously, implying that lots of EA-UFPR may disrupt the formation of β-crystal. In order to analyze the effect of EA-UFPR on crystal form quantitatively, the relative fraction of β

crystal (K_β) can be calculated according to the method mentioned in the experimental section and the results are listed in table 1. There are no obvious changes for K_β when continuously increasing the EA-UFPR content from 0 to 2 wt%, while a weak drop of K_β (about 10%) emerges when the EA-UFPR content reaches to the level of 4 wt%. Specifically, a significant decrease is seen when the rubber content reaches to 6 wt %.
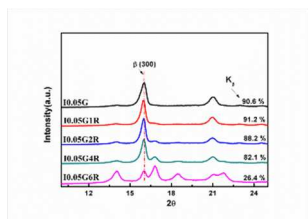
Figure 5 WAXD patterns and the relative fraction of β-crystal (K_β) of various samples taken from a cross section in the center of the injection molded bar.

Table 1 Values of X_c, K_β and K_α obtained by WAXD for samples with various EA-UFPR contents.

Samples	X_c (%)	K_α (%)	K_β (%)
I0.05G	55.5	9.4	90.6
I0.05G1R	54.8	8.8	91.2
I0.05G2R	55.2	11.8	88.2
I0.05G4R	53.8	17.9	82.1
I0.05G6R	52.2	75.4	24.6

To investigate the effects of EA-UFPR contents on non-isothermal crystallization and melting behaviour, the designed programs were carried out on DSC, as shown in Fig. 6 (a) and 6 (b). The crystallization temperatures decrease with increment in EA-UFPR content. In addition, the subsequent melting traces of various samples are presented in Fig. 6 (b). The endothermic peak appearing at about 148 ^{o}C should be associated with the melting of β-form labelled as β_1 believed as the fusion of β-form crystal initially, whereas the endothermic peak at 153 ^{o}C named as β_2 related with the fusion of perfected and/or thickened lamellae generating from partial melting and recrystallization of initial β-crystal. Besides, the peak at 162 ^{o}C (α_1) and 169 ^{o}C (α_2) of this curve are attributed to the fusion of α-crystal including primary α crystals and transformed α crystals from partial melting and recrystallization of α/β primary crystals. It is illustrated that the $T_{m-\beta1}$ changes with EA-UFPR which is related with the imperfection or thickened of lamella. The crystallinity (X_c) and relative fraction of β-crystal (K_β) are calculated quantitatively according to equations (1) and (2), as shown in Fig. 6 (c). Slight drops in K_β are seen in the second melting of samples with various EA-UFPR contents, which is inconsistent with the results in Fig. 5. In order to explore the reasons for the influences of EA-UFPR contents on K_β, the α-nucleating efficiency of EA-UFPR has been investigated, and the results are presented in supplementary materials (Fig. S1). It is found that the EA-UFPR plays no role in promoting the formation of α-crystal. However, it can induce the generation of β-crystal during machining process. On the other hand, it has been proved that the suppression effects of excessive EA-

UFPR can be removed in the second heating scans, so the decrease in K_β of I0.05G6R is related with the cooling rate during crystallization process. Hence, the competition between the nucleation role of EA-UFPR and WBG can be excluded. Therefore, the depression effects on relative fraction of β crystal result from adding excessive rubber particles are attributed to its obstruction effects on the movement of polypropylene chains.
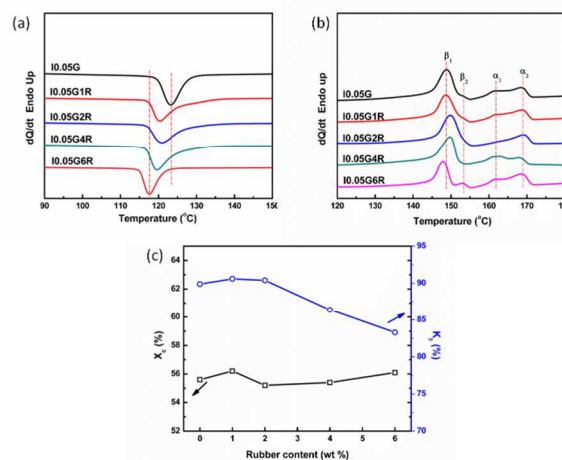
Figure 6 DSC thermograms of crystallization and melting curves for β-iPP containing various EA-UFPR concentrations. (a) Crystallization curves (cooling rate: 10 ^{o}C/min), (b) melting curves. (heating rate: 10 ^{o}C/min), (c) The crystallinity (X_c) and relative fraction of β-form (K_β) calculated from the melting curves of (b).

It has been proved that adding small amount of EA-UFPR has no effect on the polymorphic composition of β-nucleated iPP. Thus the factor of crystalline form should be excluded for the synergetic improvements in toughness and HDT by adding low amount of EA-UFPR. However, the decreased impact strength of I0.05G6R should be partially attributing to the intensely suppressed β-crystalline morphology. Besides, the dispersion of particles and crystalline morphology also plays a crucial role in determining the toughness and HDT.[27-29] Therefore, the dispersion of EA-UFPR were detected by SEM after selectively etching rubber phase, and the corresponding crystalline morphology etched by permanganate were characterized by SEM as presented in Fig. 7. The distance between EA-UFPR labelled in red point narrows gradually with the increment of EA-UFPR, while the size of EA-UFPR shows no obvious change. In terms of crystalline morphology, typical β spherulites are seen in I0.05G. However, a bundle-like structure with sharply decreased size is seen for sample with EA-UFPR, as shown in I0.05G1R, I0.05G2R and I0.05G4R. Additionally, a dominantly α phase is presented in I0.05G6R, which is in accordance with the result indicated by WAXD. As a result, it shows that the enhancement in notched Izod impact strength and HDT of I0.05G1R and I0.05G2R could be attributed to crystalline morphology change from spherulites into bundle-like crystals, and the depression of the superstructures size.

Obviously, the deteriorations of I0.05G4R and I0.05G6R are related to the suppression in β crystal content by EA-UFPR.
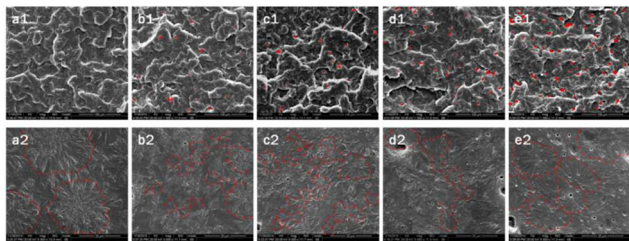
Figure 7 SEM images of various samples under different etching conditions (a) I0.05G, (b) I0.05G1R, (c) I0.05G2R, (d) I0.05G4R, (e) I0.05G6R. 1-samples were etched in xylene at 60 °C for 20 min, and the holes after removing EA-UFPR were labelled as red points in order to present more clearly. 2-samples were etched by permanganate

3.4 Effects of EA-UFPR on isothermal crystallization behaviour of β-iPP

To understand the effects of EA-UFPR on the structures of the supermolecules units of β-nucleated iPP, the isothermal crystallization behaviours of the samples were conducted by DSC (Fig. 8). With increment in EA-UFPR contents, the exotherms of β-nucleated iPP shift along the time axis. Both the induction time and the width of exotherms are increased revealing a reduction in crystallization rate with increasing EA-UFPR contents.
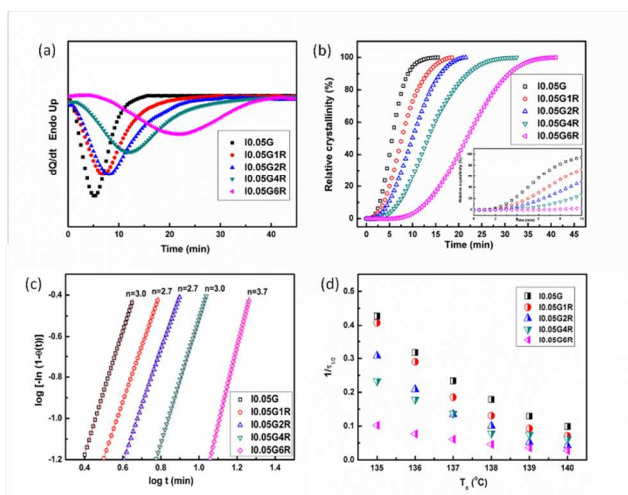
Figure 8 Effects of EA-UFPR contents on (a) DSC thermograms during isothermal crystallization process at 138 °C. (b) The responding curves of relative crystallinity versus time. (c) Avrami plot, (d) Time to attain a 50% degree of transformation ($t_{1/2}$) of β-nucleated iPP at various crystallization temperatures.

The relative degree of crystallinity at time t, $\theta(t)$, can be defined as follows:

$$\theta(t) = \frac{\theta_t(t)}{\theta_c(t_\infty)} = \frac{\int_0^t \frac{dH(t)}{dt} dt}{\int_0^{t_\infty} \frac{dH(t)}{dt} dt} = \frac{\Delta H_c}{\Delta H_\infty} \quad (6)$$

Where dH/dt is the rate of heat evolution, ΔH_c is the heat produced at time t, and ΔH_∞ is the total heat produced up to the end of crystallization. The relative crystallinity as a function of time is shown in Fig. 8 (b).

It is well known that the Avrami exponent related to the type of nucleation and to geometry of the growing crystals is critical to analysis the isothermal crystallization process.

$$\theta(t) = 1 - \exp(1 - kt^n) \quad (7)$$

Where θ is the crystalline transformation, n is the Avrami exponent, and k is the overall crystallization rate constant. The above eq 7 can also be rewritten as follows:

$$\log[-\ln(1-\theta(t)] = \log k_n + n \log t \quad (8)$$

Linear regression of these straight lines at low degrees of crystalline transformation (5-30%) yielded the Avrami parameters n (Figure 8(c)), the values obtained varies with the EA-UFPR content as follows: n≈3.0 for I0.05G, n≈2.7 for I0.05G1R, n≈2.7 for I0.05G2R, n≈3.0 for I0.05G4R, n≈3.7 for I0.05G6R. These mostly noninteger values are generally attributed to mixed growth and/or surface nucleation modes and/or two-stage crystallization. The avrami exponents exhibit no obvious changes when EA-UFPR contents are lower than 4 wt %. However, when the EA-UFPR content reaches to 6 wt %, a significant increase is obtained probably due to the mixed growth of α-crystals and β-crystals. Moreover, the heating scans after isothermal crystallized at 138 °C are exhibited in Fig. S2 (a) and the quantitative X_c and K_β are presented in Fig. S2 (b). It is found that a sharp decrease in K_β is seen in I0.05G6R, which well agrees with the results of n indicating the existence of the mixed growth of α-crystals and β-crystals at 138 °C.

Three parameters, the time of the onset of crystallization (t_{onset}) representing the induction time, time to obtain a 50% degree of crystallization ($t_{1/2}$) and the rate of crystallization ($1/t_{1/2}$) determined by the values of $t_{1/2}$ would be considered to describe the isothermal crystallization behaviour. Firstly, it is found that the time of the onset of crystallization increases with the increment in EA-UFPR content, indicating the addition of EA-UFPR is disadvantageous for the nucleation of β crystal. It is suggested that the addition of EA-UFPR weakens the ability of polypropylene chains to form stable nuclei. Secondly, it is well known that 1/ $t_{1/2}$ represents the total crystallization rate and the values are presented in Fig. 8(c).[30] Slow-downs of crystallization rate emerge after adding EA-UFPR, and the suppression effect becomes dominant with increasing the EA-UFPR content. The crystallization rate is governed by the nucleation and crystal growth, hence the formation of stable nuclei and the diffusion abilities of chain segments to the nuclei surface are the two key factors influencing the crystallization rate.[30,31] Therefore, it is proposed that the decrease in crystallization rate after adding EA-UFPR is mainly caused by two reasons: (1) the interaction between

EA-UFPR particles and the nuclei of β-nucleation, which slows down the assembly of β-nuclei to generate big nucleation spots, and (2) the obstruction effect of rubber particles on the diffusion of iPP chain.

3.5 Evolutions of crystalline morphology during isothermal crystallization

In order to explore the influence of EA-UFPR on crystalline morphology of β-nucleated iPP, the evolutions in crystalline morphologies of various samples during isothermal process were detected by polarized optical microscopy (POM). A proper crystallization temperature (T_c=138 ^{o}C) was selected and kept for 30 min to in-situ observe the crystallization process in detail as shown in Fig. 9. Micrographs of β-nucleated iPP (I0.05G) exhibit dominating β-spherulites in Fig. 9 (a). However, significant differences are seen for β-iPP after adding 1 wt % EA-UFPR. It is observed that the nucleus density in I0.05G1R (Fig. 8 (b-1 min)) significantly increases as compared with that in I0.05G (Fig. 9 (b-1 min)). In addition, needle-like crystals form in I0.05G1R, I0.05G2R and I0.05G4R. Besides, the size of the crystal bundles of β-iPP with EA-UFPR is much smaller than that of β-iPP. It is demonstrated that the addition of EA-UFPR refines the size of the superstructures because of the increment in nucleus density, and changes the crystalline morphology of β-crystals from spherulitic to needle-like type. For I0.05G6R, isolated β-spherulites surrounding with a large number of α-crystals was obtained as probably involved with hindering effect of EA-UFPR on the diffusion of iPP chains.
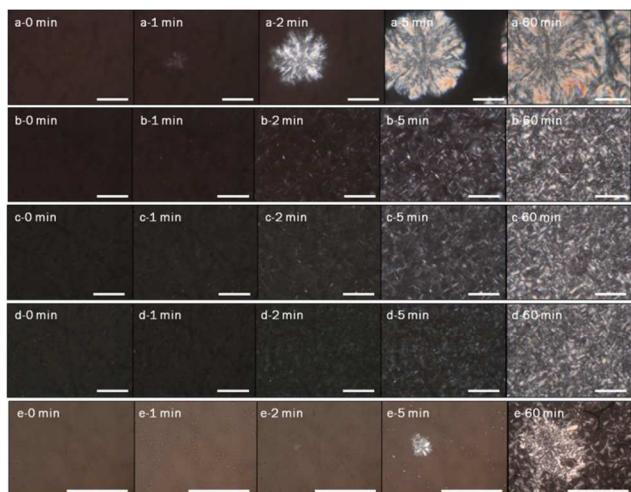
Figure 9 POM photographs showing the evolution of crystalline morphology at 138 ^{o}C (a) I0.05G, (b) I0.05G1R, (c) I0.05G2R, (d) I0.05G4R, (e) I0.05G6R. Scale bars represent 100 μm.

To obtain a better understanding of the needle-like crystal in I0.05G1R, some higher resolution micrographs of the etched samples obtained from isothermal crystallization at 138 ^{o}C for 1 min were detected by SEM as shown in Fig. 10. In order to exhibit the

structure of crystal bundles clearly, the size of the selected supermolecular units in I0.05G is smaller than most of crystals, so it is meaningless to compare the size of superstructures between I0.05G and I0.05G1R. The β-spherulites are detected in I0.05G, which are separated from each other like islands. However, it is interesting to find that interconnected crystals are obtained in I0.05G1R. The nucleation is fast since numbers of nucleations emerge simultaneously, so their growth depends on the medium of the matrix and may lead to cessation of nucleation at the later stages of crystallization. Thus, the majority of crystals grow into small-sized and imperfect bundle-like morphology. [32] The β-spherulites in I0.05G is attributed to the well solubility and subsequent high level of self-organization of WBG.[15] Nucleating agent can be partial or completely dissolved in matrix, self-assembles and induces the expitaxial growth of matrix on it as various shapes, such as spherulites, transcrystalline entity and dentrites depends on temperature[15], concentration[33], thermal conditions during cooling and crystallization[34,35]. The self-assembly process is usually driven by weak intermolecular interactions, such as Van de Waals interactions, hydrogen bonds, aromatic interactions, and electrostatic interactions. Hence, the generations of bundle-like crystals in I0.05G1R indicate that the ability of self-assembly of β-NA becomes weakened after 1wt % EA-UFPR. It is proposed that the stability of single needle-like nucleating site can be enhanced owing to its interaction with rubber particles. In consequence, numbers of bundle-like crystals induced by large amount of nucleating points are observed. It is well known that the more the connections between crystals are, the better the mechanical performance is. Hence, the formation of β-spherulite is in favor of the enhancement in mechanical properties compared with bundle-like crystals. However, totally opposite results are observed in our study due to the existence of interconnected bundle-like crystals. It has been proved that interlocked nano-fibrils bundle structure was found to have a crack-stopping property.[36, 37] From the above analysis, the bundle-like crystal in the sample with low EA-UFPR content (1 wt % ~ 2 wt %) is neighboring connected, and then, it is effective in stopping the propagation of crack preventing the brittle fracture. Therefore, the formation of interconnected bundle-like crystalline morphology in our study is beneficial for the synergistic improvement of toughness in I0.05G1R.
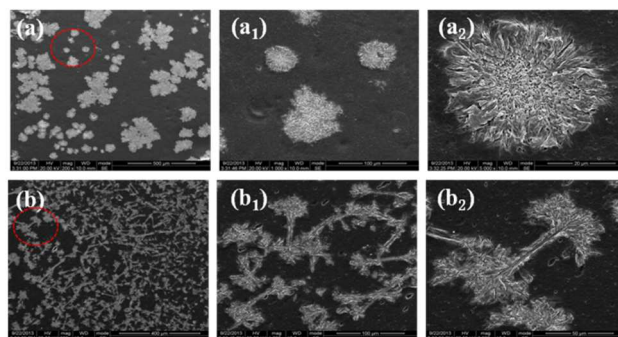
Figure 10 Typical SEM micrographs for crystalline morphology of etched samples obtained from isothermal crystallization process at 138 ^{o}C (a$_1$) I0.05G, (b$_1$) I0.05G1R and the magnifications were shown in (a$_2$), (b$_2$), respectively.

4. Conclusion

In our work, combined effects of β nucleating agent and EA-UFPR on mechanical properties, thermal property, crystallization behaviour and crystalline morphology of iPP are investigated in detail. The mechanical properties including the notched Izod impact strength and tensile toughness are significantly enhanced when adding a small amount of EA-UFPR into β-iPP, and a continuous improvement of HDT with increasing of EA-UFPR content is also observed. The crystallization kinetic of β-iPP is decreased and much decreased size of crystal bundles is obtained by adding EA-UFPR. It is tentatively proposed that the mechanical improvement could be caused by the synergistic effects of EA-UFPR and β nucleating agent on plastic deformation due to the largely decreased the superstructures size and possible formation of interconnected structure as composed of the bundle-like crystals and dispersed EA-UFPR particles.

Acknowledgements

Notes and References

College of Polymer Science and Engineering, State Key Laboratory of Polymer Materials Engineering, Sichuan University, Chengdu 610065, China. Fax: 0086-28-85405402, Tel: 028-85405402, Email: qiangfu@scu.edu.cn

1. S. V. Meille, S. Bruckner and W. Porizio, *Macromolecules*, 1990, **23**, 4114-4121.
2. A. T. Jones, J. M. Aizlewood and D. R. Beckett, *Die Makromolekulare Chemie*, 1964, **75**, 134-158.
3. F. J. Padden and H. D. Keith, *Journal of Applied Physics*, 1959, **30**, 1479-1484.
4. E. Lezak, Z. Bartczak and A. Galeski, *Polymer*, 2006, **47**, 8562-8574.
5. J. X. Li, W. L. Cheung and C. M. Chan, *Polymer*, 1999, **40**, 2089-2102.
6. Y. H. Chen, Z. Y. Huang, Z. M. Li, J. H. Tang and B. S. Hsiao, *RSC advances*, 2014, **4**, 14766-14776.
7. Y. H. Shi and Q. Dou, *Journal of Macromolecular Science Part B-Physics*, 2013, **52**, 476-488.
8. S. Zhao,Z. Cai and Z. Xin, *Polymer*, 2008, **49**, 2745-2754.
9. Y. Fujiwara, *Colloid & Polymer Science*, 1975, **253**, 273-282.
10. Y. H. Chen, Y. M. Mao, Z. M. Li and B. S. Hsiao, *Macromolecules*, 2010, **43**, 6760-6771.
11. H. Huo, S. Jiang, L. An and J. Feng, *Macromolecules*, 2004, **37**, 2478-2483.
12. L. Wang and M. B. Yang, *RSC Advances*, 2014, **4**, 25135-25147.
13. F. Luo, K. Wang, N. Ning, C. Geng, H. Deng, F. Chen, Q. Fu, Y. Qian and D. Zheng, *Polymers for Advanced Technologies*, 2011, **22**, 2044-2054.
14. F. Luo, C. Xu, K. Wang, H. Deng, F. Chen and Q. Fu, *Polymer*, 2013, **53**, 1783-1790.
15. F. Luo, C. Geng, K. Wang, H. Deng, F. Chen, Q. Fu and B. Na, *Macromolecules*, 2009, **42**, 9325-9331.
16. L. Daishuang, X. Haibing, P. Jing, Z. Maolin, W. Genshuan, L. Jiuqiang and Q. Jinliang, *Radiation Physics and Chemistry*, 2007, **76**, 1732-1735.
17. Y. Q. Liu, X. H. Zhang, G. S. Wei, J. M. Gao, F. Huang, M. L. Zhang, M. F. Guo and J. L. Qiao, *Chinese Journal of Polymer Science*, 2002, **20**, 93-98.
18. J. Wang, C. Wang, X. Zhang, H. Wu and S. Guo, *RSC Advances*, 2014, **4**, 20297-20307.
19. M. Zhang, Y. Liu, X. Zhang, J. Gao, F. Huang, Z. Song, G. Wei and J. Qiao, *Polymer*, 2002, **43**, 5133-5138.
20. Q. Zhao, Y. Ding, B. Yang, N. Ning and Q. Fu, *Polymer Testing*, 2013, **32**, 299-305.
21. Y. Zhu, F. Luo, H. Bai, K. Wang, H. Deng, F. Chen, Q.Zhang and Q. Fu, *Journal of Applied Polymer Science*, 2013, **129**, 3613-3622.
22. Y. Gao, G. Y. Zong, H. W. Bai and Q. Fu, *Chinese Journal of Polymer Science*, 2014, **32**, 245-254.
23. A. M. Díez-Pascual and M. Naffakh, *ACS Applied Materials & Interfaces*, 2013, **5**, 9691-9700.
24. D. Jarus, A. Scheibelhoffer, A. Hiltner and E. Baer, *Journal of Applied Polymer Science*, 1996, **60**, 209-219.
25. S. Xie, S. Zhang, F. Wang, H. Liu and M. Yang, *Polymer Engineering & Science*, 2005, **45**, 1247-1253.
26. M. T. Takemori, *Polymer Engineering & Science*, 1979, **19**, 1104-1109.
27. H. Bai, H. Xiu, J. Gao, H. Deng, Q. Zhang, M. Yang and Q. Fu, *ACS Appled Materials & Interfaces,* 2012, **4**, 897-905.
28. B. Na, R. Lv, S. Zou, Z. Li, N. Tian and Q. Fu, *Macromolecules*, 2010, **43**, 1702-1705.
29. C. Geng, Y. Zhu, G. Yang, Q. Fu, C. Zhang, K. Wang and T. Zhou, *Chinese Journal of Polymer Science,* 2014, **32**, 9-20.
30. S. Gupta, X. Yuan, T. C. M. Chung, M. Cakmak and R. A. Weiss, *Polymer,* 2014, **55**, 924-935.
31. J. H. Chen, B. X. Yao, W. B. Su and Y. B. Yang, *Polymer*, 2007, **48**,1756-1769.
32. P. G. Vekilov, *Crystal Growth & Design,* 2010, **10**, 5007-5019.
33. H. W. Bai, W. Y. Zhang, H. Deng, Q. Zhang, Q. Fu, *Macromolecules,* 2011, 44, 1233−1237.
34. J. Varga, A. Menyhard, *Macromolecules,* 2007, **40**, 2422-2431.
35. S. Yang, H. N. Yu, F. Lei, J. Li,*S. Y. Guo, H. Wu,*J. B. Shen, Y. Xiong, *R. Chen Macromolecules,* 2015, DOI: 10.1021/acs.macromol.5b00396
36. G. Xu, L. Gong, Z. Yang and X. Y. Liu, *Soft Matter*, 2014, **10**, 2116-2123.
37. H. R. Yang, J. Lei, L. Li, Q. Fu and Z. M. Li, *Macromolecules*, 2012, **45**, 6600-6610.

RSC Advances Accepted Manuscript